Geophysical Prospecting

EAGE EUROPEAN ASSOCIATION OF GEOSCIENTISTS & ENGINEERS

Geophysical Prospecting, 2015, **63**, 192–210 doi: 10.1111/1365-2478.12151

Signal detectability of marine electromagnetic methods in the exploration of resistive targets

Mark Goldman[1], Vladimir Mogilatov[2], Amir Haroon[3], Eldad Levi[1] and Bülent Tezkan[3]

[1]*Geophysical Institute of Israel, Lod 71100, Israel,* [2]*Institute of Petroleum Geology and Geophysics, Novosibirsk 630090, Russia, and* [3]*University of Cologne, Cologne D-50923, Germany*

Received April 2013, revision accepted February 2014

ABSTRACT

We compare selected marine electromagnetic methods for sensitivity to the presence of relatively thin resistive targets (e.g., hydrocarbons, gas hydrates, fresh groundwater, etc.). The study includes the conventional controlled-source electromagnetic method, the recently introduced transient electromagnetic prospecting with vertical electric lines method, and the novel marine circular electric dipole method, which is still in the stage of theoretical development. The comparison is based on general physical considerations, analytical (mainly asymptotic) analysis, and rigorous one-dimensional and multidimensional forward modelling. It is shown that transient electromagnetic prospecting with vertical electric lines and marine circular electric dipole methods represent an alternative to the conventional controlled-source electromagnetic method at shallow sea, where the latter becomes less efficient due to the air-wave phenomenon. Since both former methods are essentially short-offset time-domain techniques, they exhibit a much better lateral resolution than the controlled-source electromagnetic method in both shallow sea and deep sea. The greatest shortcoming of the transient electromagnetic prospecting with vertical electric lines and marine circular electric dipole methods comes from the difficulties in accurately assembling the transmitter antenna within the marine environment. This makes these methods significantly less practical than the controlled-source electromagnetic method. Consequently, the controlled-source electromagnetic method remains the leading marine electromagnetic technique in the exploration of large resistive targets in deep sea. However, exploring laterally small targets in deep sea and both small and large targets in shallow sea might require the use of the less practical transient electromagnetic prospecting with vertical electric lines and/or marine circular electric dipole method as a desirable alternative to the controlled-source electromagnetic method.

Key words: Marine electromagnetics, Signal detectability, Resistive targets.

INTRODUCTION

Over the last decade, marine geoelectromagnetic investigations have experienced a rebirth mainly due to a number of successful applications in the offshore hydrocarbon exploration (e.g., Ellingsrud *et al.* 2002; Edwards 2005; Constable and Srnka 2007; Constable 2010). In the framework of these investigations, great efforts were paid to theoretical studies of the electromagnetic (EM) fields in the presence of thin resistive layers in a conductive environment that approximated hydrocarbon reservoirs within saline-water-saturated sub-seafloor sediments. These developments in turn

E-mail: mark@gii.co.il

led to numerous comprehensive studies of the EM fields in complicated marine environments both in the frequency and time domains (e.g., Weiss and Constable 2006; Chave 2009; Um *et al.* 2012; Singer and Atramonova 2013).

Among all marine EM methods, the undisputed leader is the controlled-source EM (CSEM) method mainly due to its exceptional signal detectability with regard to resistive sub-seafloor targets and practical feasibility using in-line horizontal electric dipoles (HEDs) (Chave and Cox 1982). The superior detectability of the CSEM method is based on a specific propagation phenomenon, which takes place under certain geoelectric conditions and parameters of the CSEM system located at the sea floor. Under these conditions, most of the EM energy travels from a transmitter to a receiver through sub-seafloor resistive structures ("guided waves", Weidelt 2007). It is interesting to note that this phenomenon was discovered simultaneously and independently and both empirically and theoretically. Cox (1981) reported the successful use of the long-offset (up to some 18 km long) CSEM system at frequencies near 1 Hz to study the conductivity of the crust near the East Pacific Rise. Kaufman *et al.* (1981) described the physical basics of the propagation phenomenon supported by the appropriate forward modelling for a pure transverse electric (TE) mode Ex–Bz CSEM system. It was shown that, due to the guided propagation effect, the signal detectability of a vertical magnetic dipole (VMD) increases by orders of magnitude compared to conventional low induction numbers (LIN) methods, in which resistive targets are barely detectable. A further comprehensive study carried out by Chave and Cox (1982) for different transmitter–receiver (Tx–Rx) configurations allowed finding the most efficient CSEM array, including in-line Ex–Ex electric dipoles in the frequency domain. This array has formed the basis of the majority of modern CSEM systems successfully applied in the offshore hydrocarbon exploration.

In order to overcome the inherent problems of the conventional CSEM system caused by the airwave effect (shallow sea problem) and by the long offsets used (low lateral resolution), alternative short-offset time-domain methods have been investigated during the last years (e.g., Cuevas and Alumbaugh 2011; Um *et al.* 2012). One of such systems employing vertical electric lines (VELs) as both transmitter and receiver has been successfully tested in the field (Holten *et al.*, 2009).

This article is devoted to a comparative study of selected marine EM methods, which exhibit an increased sensitivity to the presence of relatively thin sub-seafloor resistive targets (e.g., hydrocarbons, gas hydrates, fresh groundwater, etc.). The study is based on the use of analytical (mainly asymptotic) expressions, rigorous forward one-dimensional (1D) and multidimensional modelling, and some relevant field examples. It is focused on studying a single, but to our mind, the most basic feature of geophysical methods, namely, the ability to distinguish a measured signal caused by the target and a signal caused by a surrounding medium (sometimes called geological noise). Such ability is called hereafter the detectability of a method. Quantitatively, it is represented by the relative target response defined as a ratio of the measured (calculated) signal in the presence of a target(s) to that without it (them). It is clear that sufficiently high detectability represents only a necessary but not a sufficient condition for an accurate quantitative delineation of the target. Other important issues, such as signal-to-noise ratio (SNR), non-uniqueness of the inversion, etc., have been left beyond the scope of this article.

Our priority in choosing detectability as a decisive factor was dictated by a simple fact: If a method demonstrates a prohibitively low detectability, then the rest of the issues become irrelevant. If, on the contrary, the method exhibits sufficiently high detectability, the other problems can still be treated in different ways. It should be noted that the discussed detectability is closely related to a more common feature called resolution or resolving power of a method. In some cases, these features are very similar, if not identical. For example, in the case of a single target, a lateral or vertical resolution is normally estimated by the target response for minimum measurable lateral and vertical dimensions of the target, respectively. In this case, the detectability and the resolution are very similar, if not have identical features. However, in the case of, for example, two or several adjacent (either laterally or vertically) targets, the high overall target response does not necessarily mean the ability to resolve the targets separately, although it does represent the necessary condition for the latter. In other words, the targets can be clearly detected but, at the same time, hardly separated (resolved) from each other. For example, discriminating highly resistive anhydrite layers from underlying hydrocarbons might represent a much more difficult exploration problem than just detecting them.

In the course of this study, we compared three different methods, the choice of which was solely dictated by their high detectability of sub-seafloor resistive structures. The main output of the study was thus formulating the optimum conditions for the application of each method.

The selected methods are:

(i) CSEM (e.g., Constable 2006);
(ii) transient EM prospecting with VELs (TEMP-VEL) (Holten *et al.* 2009);

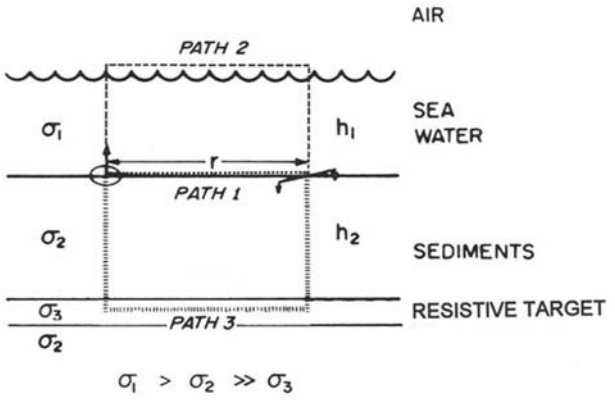

Figure 1 Schematic explanation of the CSEM phenomenon. Under the conditions described in the paper, most of the energy from the transmitter propagates to the receiver through path 3. The shown Tx–Rx configuration (Ex–Bz) produces a unimodal TE response. In practice, the more efficient in-line Ex–Ex configuration is mostly used. The picture reproduces chronologically the first substantiation of the CSEM phenomenon (Kaufman *et al.* 1981).

(iii) marine circular electric dipole (MCED) soundings (a novel application of technology based on the use of a CED transmitter developed by Mogilatov (1992, 1996) and Mogilatov and Balashov (1996)).

The term CSEM is used hereafter for the specific essentially long-offset frequency-domain method, whereas the other two methods are short-offset time-domain techniques.

METHODS

Controlled-source electromagnetic

Depending on frequency and Tx–Rx offset (r), the signal in the frequency domain belongs to the following two asymptotic ranges:

- *Low induction numbers (LIN)* with $|k|r < 1$
- *High induction numbers (HIN)* with $|k|r > 1$,

where $k = \sqrt{i\omega\mu\sigma}$ is the wavenumber. The value of conductivity σ is selected the largest for the LIN range and the lowest for the HIN range excluding the target. In the model under consideration (Fig. 1), $\sigma = \sigma_1$ in the LIN range, and $\sigma = \sigma_2$ in the HIN range.

In the LIN range, the target response is similar to that in the direct current (DC) limit. The amplitude of the signal decays as a power of distance both within the subsurface and in the air; therefore, it does not dramatically depend on the depth of the sea. As a result, the CSEM method in the LIN range can be in principle applied both in shallow sea and deep sea.

The behaviour of the CSEM signal in the HIN range is entirely different. In this range, the signal decays exponentially ($e^{-|k|L}$) with a distance L in the conductive medium and as a power of a distance in the air and within any high resistivity (strictly speaking, insulating) structure in the Earth. As a result, depending on the geometry (Fig. 1), the signal in the HIN range might propagate mainly through the resistive target rather than through the air. The sufficient conditions for such propagation are $r \gg h_1 > 2h_2$, but they could be less restrictive depending on the conductivity contrasts σ_1/σ_2 and/or the specific Tx–Rx array used. Under the above conditions, most of the EM energy will propagate through the target, provided the latter is highly resistive. The energy propagating through all other possible paths is much more attenuated than that one arriving through the target. Weidelt (2007) called this phenomenon guided wave propagation.

Although the amplitudes of the signals are exponentially small and, as a result, the overall SNR is also small, the part of the signal arriving through the target under the above-mentioned conditions is the largest one. This provides a relatively high target response and, accordingly, the well-known high-signal detectability of the CSEM method.

It should be noted that the above physical considerations are applicable to both TE and transverse magnetic (TM) fields. In fact, the propagation phenomenon realized in the CSEM method was physically described and numerically substantiated for the first time by Kaufman *et al.* (1981) for a unimodal TE field as shown in Fig. 1. The use of bimodal HEDs and/or of unimodal TM vertical electric dipoles (VEDs) leads to a further increase in the relative target response. However, the initial cause of the high detectability of the CSEM method is the above-described guided propagation phenomenon. If the conditions of the phenomenon are violated (shallow sea, short offsets, and very low frequencies), the CSEM response loses its exceptionally high detectability in the case of either bimodal or even unimodal TM fields and becomes completely insensitive to resistive structures in the case of a unimodal TE field. If contrary, the above conditions are held, even a unimodal TE field provides a reasonably high relative target response (Kaufman and Keller 1983; Goldman 1987), although it is much smaller than that of the TM field under similar conditions. Calculations show that the propagation phenomenon enhances signal detectability compared with the LIN limits in both TE and TM modes at approximately the same rate. As a result, thin resistive layers, which are completely missed by TE fields in the LIN range, might become detectable

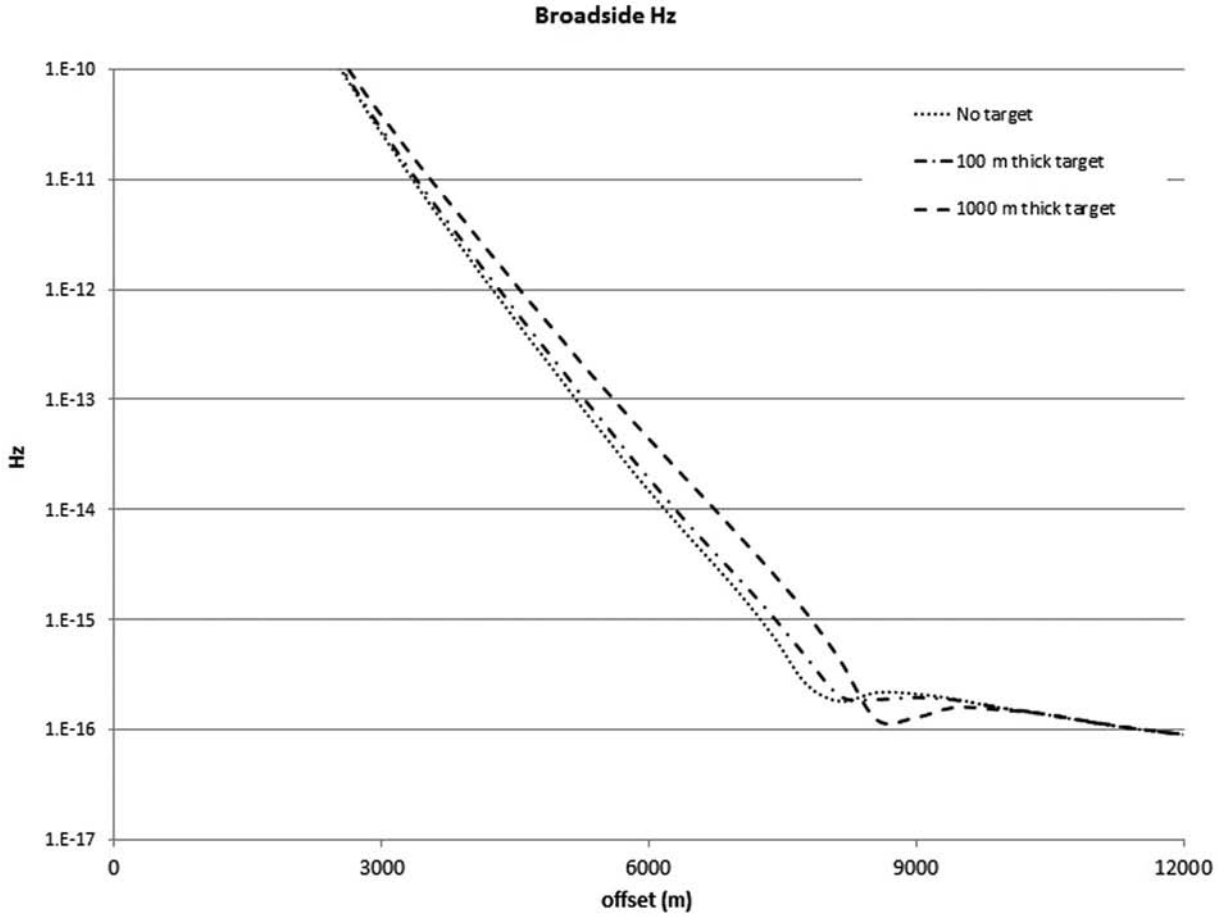

Figure 2 Amplitudes of broadside Ex–Hz responses for the canonical marine geoelectric model shown in Fig. 1. The field amplitude, Hz, is in ampere per meters normalized by the transmitter moment. The index of the curves is the thickness of the resistive layer. Rho1 = 0.33 Ωm, rho2 = 1 Ωm, and rho3 = 100 Ωm; h1 = 2000 m, h2 = 1000 m, and h3 varies from 0 to 1000 m. The Tx–Rx array is located at a depth of 1975 m (25 m above the sea bottom). The frequency is 1 Hz.

under the above-discussed "propagation conditions." Figure 2 shows such signals for both thin and thick resistive targets. One can see that even the thin layer provided some 75% relative target response, whereas such target would be completely undetectable if the guided propagation conditions are violated (i.e., at the LIN range and/or at shallow sea and/or at the sea surface). Since the airwave effect is more crucial for TE fields, the calculations were carried out for deeper sea (2-km depth) instead of 1-km-deep sea used in the analysis of electric fields.

It should be emphasized that the TE field is considered here not because it provides particularly high detectability but rather because it more clearly demonstrates the influence of the guided propagation effect. Indeed, the latter is the only cause for detectability of the TE field, whereas in the case of the unimodal TM field or bimodal TE–TM field, the effect is superimposed on their inherent LIN detectability.

TEMP-VEL

Since the term TEMP-VEL is reserved for the specific system utilizing VELs (VEDs) as both transmitter and receiver antennae, the more general term VED or VEL will be used in the course of this study for arbitrary receiver antennae.

Although the principal possibility of using VELs or VEDs both in frequency and time domains has been discussed since 1961 (Nazarenko 1961; Edwards, Law, and DeLaurier 1981; Chave and Cox 1982), this did not result in a general theoretical acceptance or commercial development of the appropriate methods. This is partially explained by extraordinary difficulties in assembling strictly VEDs (VELs) either in boreholes or in the sea, and this limitation is particularly crucial for delineating resistive targets. Some publications also testified to a lower resolution of VEDs compared with HEDs (see the work

of Key (2009) for the frequency domain and the work of Um *et al.* (2012) for the time domain).

In the frequency domain, the method was investigated and practically applied mainly in the so-called MOSES system (Edwards *et al.* 1985) based on the measurements of a horizontal magnetic field at very low frequencies belonging to the LIN range. In this range, the sensitivity of the signal to sub-seafloor thin resistive layers is fairly low; therefore, the MOSES method did not become prominent in the offshore hydrocarbon geophysical exploration. It should be noted that the sensitivity of the MOSES-like system could be greatly increased if the measurements were carried out in the HIN range under the above-described guided mode conditions. Weidelt (2007) and Loseth and Amundsen (2007) showed that, under these conditions, TM fields in general and, as such, horizontal magnetic and electric fields of VEDs, in particular, are extremely sensitive to resistive layers. In fact, they are even more sensitive than the existing bimodal conventional Ex–Ex CSEM system. However, from a practical point of view, the application of any VED system, either MOSES-like or those using electrical dipoles, does not seem practically justified in the HIN range compared with the conventional CSEM using in-line HEDs, i.e., Ex–Ex. Indeed, the conventional CSEM provides sufficiently high target detectability and, in addition, is incomparably more practical than long-offset VED systems. Therefore, the use of the latter only because of their potentially higher detectability does not seem well justified. It is also worth to note that, despite higher detectability, a vertical electric field might exhibit lower resolution than, for example, Ex–Ex in recovering a thin resistor (Key 2009).

The situation is completely different in the time domain, where VED fields at short offsets become highly sensitive to thin resistive layers in both shallow sea and deep sea. Cuevas and Alumbaugh (2011) showed high signal detectability of short-offset VED fields based on rigorous 1D modelling, physical considerations, and some asymptotic mathematical analysis. In the following, we present an alternative asymptotic analysis, which clearly emphasizes a potentially very high detectability and resolution of the VED fields in the presence of highly resistive structures.

Similar to all other systems, the theoretical study of VED fields began by using the simplest possible geoelectric models of a half-space or that of two conductive half-spaces. These are the only models for which the solution is represented analytically and the solution for VEDs is very similar to that of conventional HEDs and both horizontal and vertical magnetic dipoles. At sufficiently late times after the transmitter current has been switched off, the electrical field decays with

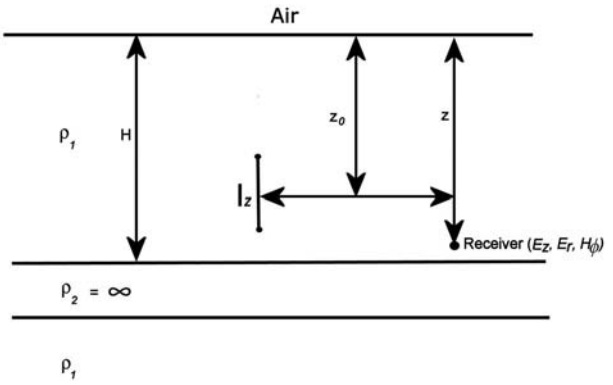

Figure 3 The basic half-space model including an insulating layer.

time as $t^{-5/2}$ and is proportional to the conductivity of the half-space in the power of 3/2 (e.g., Goldman 1990; Singer and Atramonova 2013). This similarity along with the rapid attenuation in low dissipation rocks and, thus, much weaker VED signals compared with those from all other sources led to the conclusion that the main feature of VEDs is a significantly lesser penetration depth (e.g., Chave and Cox 1982). Additionally, taking the much more complicated field setup of VED systems into account, it is no wonder that the latter did not gain much popularity in offshore geophysical exploration.

The situation becomes entirely different if the basic analysis of VED fields is carried out for a half-space model including a resistive layer (Fig. 3). To understand the difference, one has first to obtain an analytical solution for such model. Although it is not available in the entire time range and/or for an arbitrary resistivity of the layer, very important information can be obtained from the limiting case of an insulating layer at late times, which allows an analytical solution in elementary functions. In order to obtain such a solution, it is convenient to formulate the boundary value problem directly in the time domain.

Such an approach is not very common in the geophysical literature, where most of the solutions for VEDs and other controlled-source time-domain methods are commonly obtained in the frequency domain followed by the inverse Fourier transform into the time domain. Although this method also allows obtaining an analytical asymptotic solution at late times by changing the order of integration between the Bessel and Fourier integrals and by locating poles of the integrand in the complex plane of ω (e.g., Goldman and Fitterman 1987), the direct time-domain solution to the boundary value problem is much more elegant. It was first introduced by Tikhonov (1950), but unfortunately, it was abandoned in further studies, partly because it is limited to models with an ideally

insulating or perfectly conducting basement. An example of the Tikhonov's approach applied to a VED source within a conductive slab is given in Appendix A. It is quite clear from both physical and mathematical considerations that, in the quasistatic case, the Tikhonov's slab model is equivalent to the model with a finite thickness of the insulating basement, as shown in Fig. 3. This follows from the toroidal current distribution above an insulating layer that prevents the appearance of a magnetic field below it and from the zero's boundary condition for the magnetic field on the top of an insulating layer of an arbitrary thickness.

The solutions are different if displacement currents are taken into account, but this subject is beyond the scope of this article.

By using equations (A7) for the model shown in Fig. 3 and by increasing normalized time $\bar{t}$, one can see that the influence of the terms with index $k \geq 2$ decreases, and the transient response at sufficiently late times exponentially decays as a function of $\bar{t}$, i.e.,

$$H_\varphi = \frac{I_z}{\pi H^2}\exp(-\pi^2\bar{t})\sin(\pi\bar{z})\int_0^\infty R_1\exp(-\lambda^2\bar{t})\lambda J_1(\lambda\bar{r})d\lambda \quad (1)$$

$$E_r = -\frac{I_z\rho_1}{H^3}\exp(-\pi^2\bar{t})\cos(\pi\bar{z})\int_0^\infty R_1\exp(-\lambda^2\bar{t})\lambda J_1(\lambda\bar{r})d\lambda \quad (2)$$

$$E_z = \frac{I_z\rho_1}{\pi H^3}\exp(-\pi^2\bar{t})\sin(\pi\bar{z})\int_0^\infty R_1\exp(-\lambda^2\bar{t})\lambda^2 J_0(\lambda\bar{r})d\lambda. \quad (3)$$

A further increase in the normalized time allows expanding R_1 in powers of λ. Then, neglecting the terms above the second order, one obtains the following simple asymptotical expressions for the field components:

$$H_\varphi = \frac{I_z}{4\pi^3 H^3}r\exp(-\pi^2\bar{t})\sin(\pi\bar{z})L \quad (4)$$

$$E_r = \frac{I_z\rho_1}{4\pi^2 H^4}r\exp(-\pi^2\bar{t})\cos(\pi\bar{z})L \quad (5)$$

$$E_z = \frac{I_z\rho_1}{2\pi^3 H^3}\exp(-\pi^2\bar{t})\sin(\pi\bar{z})\left(1-\frac{\bar{r}^2}{4\bar{t}}\right)L, \quad (6)$$

where $L = \dfrac{\sin(\pi\bar{z}_0)}{\bar{t}^2}\exp-\dfrac{\bar{r}^2}{4\bar{t}}$, $\bar{t} = \dfrac{t}{\mu_0\sigma_1 H^2}$, $\bar{r} = \dfrac{r}{H}$, $\bar{z} = \dfrac{z}{H}$, $\sigma_1 = \dfrac{1}{\rho_1}$.

A comparison with rigorous calculations shows that equations (1)–(3) are valid starting from $\bar{t} > 0.2$ and equations (4)–(6) are valid starting from $\bar{t} > 15$ (with a 5% error for all the equations). Thus, the above equations show that, contrary to all other transient EM (TEM) systems available, only the VED fields exponentially depend on time and on all geoelectric parameters of the model. This is also true for an arbitrary number of layers above an insulating layer (Goldman 1990). The benefit of such peculiarity is clear: At least theoretically, the detectability of the method, as well as the resolution regarding geoelectric parameters of the model above the insulating layer, is unlimited. Let us consider, for example, the resolution of the Er component with regard to the depth to the insulating layer. For this, let us compare the responses from two models with different depths, i.e., H_1 and H_2. According to (5), the ratio of the responses at sufficiently late times is proportional to $e^{(-\pi^2\frac{t}{\mu_0\sigma_1}(\frac{1}{H_1^2}-\frac{1}{H_2^2}))}$, i.e., infinitely increases/decreases with time. This means that, theoretically, VEDs can resolve any small variations in the depth to the target if the latter is represented by an insulating layer of arbitrary thickness. These idealized analytical considerations will be supported in the following by rigorous calculations for finite resistivities.

In the case of conventional arrays, which do not include VEDs as a transmitter or receiver, the response for the model in question is proportional to the longitudinal conductance ($\sigma_1 H$) of the half-space above the target in powers of 2 or 3 depending on the array (Kaufman and Keller 1983). Therefore, the ratio of the responses for different target depths at sufficiently late times is a constant value proportional to the ratio of the depths in the appropriate power (2 or 3). This means that, even theoretically, the resolution of conventional transient systems with regard to the depth to the target is limited by some threshold value, which is dictated by geological noise in the area. Above all, contrary to VEDs, the responses of conventional arrays at late times depend on the total longitudinal conductance above the target and not on the required resistivity and depth to the target separately.

A similar asymptotic behaviour at late times takes place in arbitrary 1D Earth above an insulating layer. In such a model, VED responses exponentially depend on all geoelectric parameters separately, whereas the responses for conventional arrays depend on the total longitudinal conductance of the medium above an insulating layer in the appropriate powers of 2 or 3 (Goldman and Mogilatov 1978; Goldman 1990).

It is clear that the above considerations, which are strictly valid only under idealized conditions (insulating target and very late times), should be examined for real resistivity and times. For comparison, Figs. 4 and 5 show the VED and HED responses, respectively, for the canonical marine model

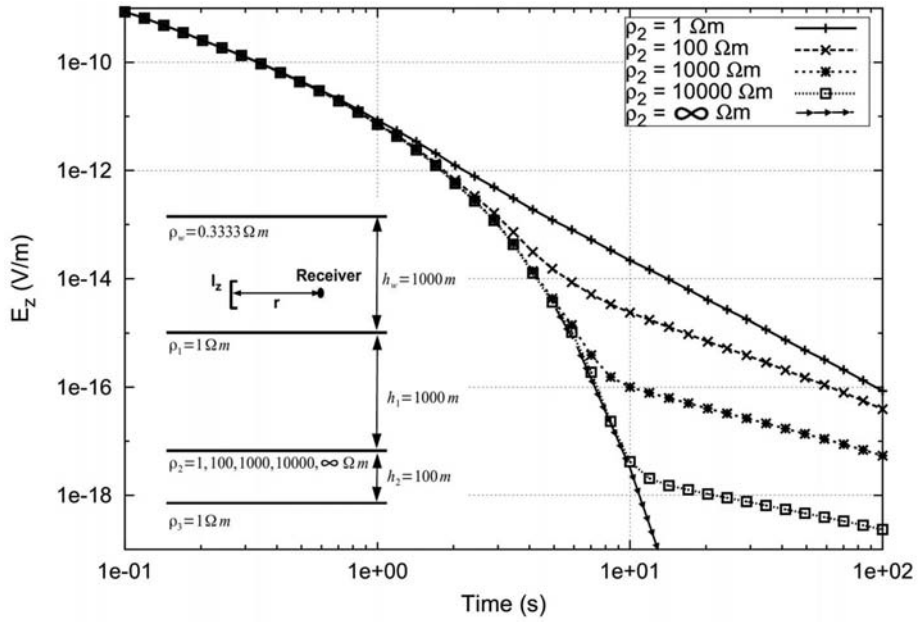

Figure 4 Transient responses of a short-offset ($r = 100$ m) Ez–Ez array for different resistivity of the target layer. The detectability of the insulating layer unlimitedly increases with time. In the case of a finite resistivity of the target, the detectability forms a maximum at a certain time, which increases with the resistivity. The responses are excellently resolved with regard to the resistivity of the target.

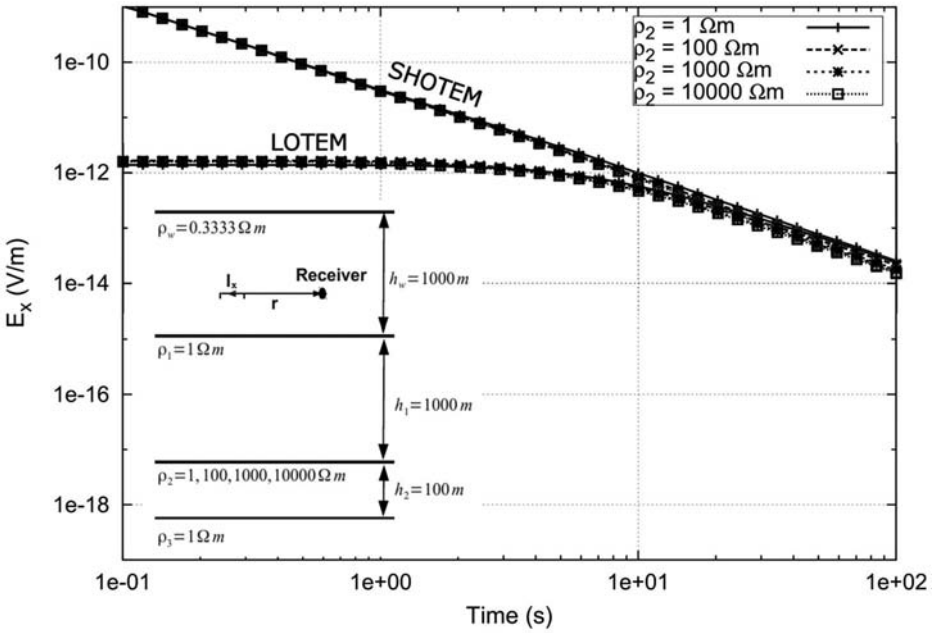

Figure 5 Transient responses of the SHOTEM ($r = 100$ m) and LOTEM ($r = 5000$ m) in line Ex–Ex array for different resistivities of the target layer.

including a resistive layer of variable resistivity. The calculations were cross-checked by using our own 1D forward modelling code and the one written by Carsten Scholl (personal communication).

It is important to emphasize that the exceptional resolving power of short-offset time-domain VED systems with regard to all geoelectric parameters of arbitrary 1D models above an insulating layer is caused by its exponential (more precisely,

quasiexponential) dependence on the above parameters. As a result, VED systems resolve equally well both thin resistive and thin conductive layers (Goldman 1990). In the frequency domain, where the quadrature component of the field in the LIN range is proportional to the longitudinal conductance of the model above the insulating layer, the resolving power of VEDs is entirely different and, in most cases, similar to that of conventional non-VED systems. As for the amplitude or in-phase component of the signal, they approach a DC level in the LIN range and, as a result, provide high detectability at large offsets (Goldman 1990). The highest detectability frequency-domain VED systems demonstrate under the above-mentioned guided mode conditions (e.g., Weiss and Constable 2006; Um and Alumbaugh 2007; Weidelt 2007). Nevertheless, under these conditions, a conventional Ex–Ex CSEM system also provides high detectability (in deep sea) and is far more practical and overall more efficient than any other long-offset system either in the frequency domain or the time domain. Therefore, only the short-offset transient VED system is discussed here as a possible alternative to the conventional Ex–Ex CSEM method, when the propagation conditions are violated. It should be noted that the extremely short offsets used for the calculations throughout this paper mainly affect the SNR, which is not considered in this study. In practice (e.g., Holten *et al.* 2009), much larger offsets are used to improve the SNR. An inevitable tradeoff between SNR and, for example, lateral resolution should be analyzed in each case.

For comparison, Fig. 5 shows short-offset TEM (SHOTEM) and long-offset TEM (LOTEM) transient responses using in-line Ex–Ex configuration for the same model shown in Fig. 4. It can be seen that, at late times, Ez–Ez (Fig. 4) provided significantly higher detectability than both SHOTEM and LOTEM Ex–Ex arrays. At early times, only the LOTEM Ex–Ex configuration provided some (fairly low) detectability, which is identical to that of the dipole–dipole DC method. In addition to detectability, the VED fields demonstrated an exceptionally high resolution with regard to the target resistivity. This feature could be crucial for discriminating the target (e.g., hydrocarbons) from the geologic noise (e.g., anhydrites, magmatic rocks, etc.). The resolution of short-offset VED systems to the rest of the geoelectric parameters strongly depends on the resistivity of the target or, alternatively, of any resistive structure below (e.g., basalts, anhydrites, etc.). The larger the resistivity, the higher the resolution.

At first glance, the above observations contradict the conclusions drawn by Um *et al.* (2012) in their comprehensive study of short-offset transient electric fields of VEDs in 3D marine environments. According to Um *et al.* (2012), due to the lack of the propagation phenomenon (guided mode) at short offsets, VED fields lack signal detectability as well. This inconsistency is apparently caused by the insufficiently late time range considered by Um *et al.* (2012). Due to practical considerations (a limited receiver noise level), their calculations were carried out up to roughly 5 s. Figure 4 shows that, in such time range, the VED field indeed does not show significant detectability.

In conclusion, it is interesting to note that the behavior of VED fields above an insulating layer is similar to that of TE fields in the presence of local conductors within an insulating medium. In both cases, the fields exponentially depend on geoelectric properties of the target at late times. In contrast, the fields are simply proportional to conductivity and squared dimensions of the target in the frequency-domain LIN range. This difference leads to significantly higher resolving power of the above transient systems with regard to geoelectric parameters of the respective targets compared with identical systems in the frequency domain (Kaufman 1978).

These observations contradict a fairly common opinion that no principal difference exists between frequency-domain and time-domain measurements since, mathematically, they can be Fourier/Laplace transformed into each other. This opinion exists despite the appearance of various comprehensive comparative studies, which do testify to the considerable practical difference between the domains (e.g., Kaufman 1978; Connel and Key 2013). The above-mentioned superior resolution of the short-offset time-domain response over the appropriate response in the frequency domain is caused by the basic difference between the responses in asymptotic limits. This difference cannot be bridged by applying the numerical Fourier/Laplace transform to the frequency-domain field data because one has to obtain an exponentially small response at late times by a summation of relatively large sign varying numbers in the frequency domain. This procedure is numerically unstable, and there is always a sufficiently large time instant, after which the numerical Fourier/Laplace transform of real frequency-domain data fails irrespective of what specific numerical algorithm has been used for the transform. For example, comparison of different highly accurate numerical quadrature algorithms (e.g., Filon-type quadratures) showed instability in transformation of synthetic frequency-domain data at those times, when the signal dropped by some five to six orders of magnitude below the initial value (Goldman 1983).

It is possible to obtain more stable and computationally efficient transformations from the frequency domain to

the time domain using non-orthogonal basis functions, whose Fourier transforms are analytic, rather than through direct numerical transforms using continuous sine functions orthogonal over the periodic time measurement (Holladay 1981; Stolz and Macnae 1998).

It should be noted that the above observations are generally valid only for a step-off current waveform in the time domain and for a standard sinusoidal current waveform in the frequency domain. The comparison carried out by Connell and Key (2013) for a step-on and impulse time-domain Tx waveforms and various practically available frequency-domain CSEM waveforms led to the opposite conclusion that the time-domain response for the canonical model shown in Fig. 1 has lower resolution than that in the frequency domain. Since a step-on waveform is inapplicable in short-offset time-domain EM (TDEM) method with electrical dipoles, such waveform is not considered in this study.

The above-discussed advantages of the time-domain VED systems are severely deteriorated by an inevitable non-verticality of the systems both on land (in boreholes) and in the sea. Contrary to geometrical errors in the conventional systems (e.g., Ex–Ex), which are generally proportional to the sine/cosine of the angle shift, the appearance of the parasitic horizontal electric field might produce huge errors due to either the transmitter or the receiver VED inclination. This is because horizontal electric fields decay much slower than the required Ez at late times. In order to somehow reduce the geometrical errors, the first practical marine VED system comprises two VEDs (lines), i.e., it is the Ez–Ez system (Holten *et al.* 2009). Contrary to, for example, Ez–Ex arrays, in which the signal from the parasitic HED transmitter is picked up by the real HED receiver, in the Ez–Ez array, both transmitter and receiver HEDs are parasitic and thus have a very small moment. However, due to the power-law decay of the signal at late times, even very small parasitic HEDs will produce significant errors at sufficiently late times. Therefore, the above-mentioned Ez–Ez system, which is the VED system least sensitive to geometrical errors (Holten *et al.* 2009; Um *et al.* 2012), could be still inappropriate for real measurements under certain conditions. These conditions are studied numerically in Appendix B.

In addition to the above-discussed signal detectability and resistivity resolution, short-offset transient VED systems are expected to have a sufficiently high lateral resolution as well. This feature is typical for all SHOTEM systems compared with, for example, LOTEM or CSEM systems. The detailed quantitative study of lateral resolution based on more realistic multidimensional models and a finite resistivity of the basement will be carried out in the modelling section.

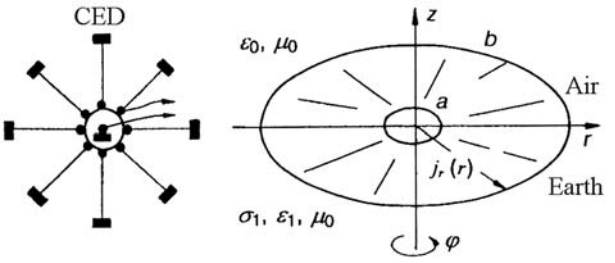

Figure 6 The "real" (left) and the "ideal" (right) CEDs comprising two concentric electrode systems discretely or continuously distributed along the circles of radius a (the inner or central electrode(s)) and b (the outer electrode(s)), respectively.

Marine circular electric dipole

The above-discussed exceptional features of the time-domain VED systems, on one hand, and the necessity to use deep boreholes to apply such systems on land, on the other hand, led to the development of a horizontal analogue of VEDs called CED. The method was first introduced and theoretically substantiated by Mogilatov (1992) and further developed and practically realized by Mogilatov and Balashov (1996). The method comprises the entirely new source of the primary field, which includes a central electrode connected to one pole of a generator and (theoretically) a continuum of electrodes located along a circle and connected to another pole (Fig. 6). Of course, in practice, the number of outer electrodes is finite and, in most cases, adequately represents the ideal CED if the number of the outer electrodes ≥ 8 (Mogilatov and Balashov 1996).

The rigorous solution to the 1D boundary value problem for the radial current sheet source in the frequency domain (Mogilatov 1996; J. Wait personal communication) shows that the EM field of CED located at the surface of the Earth exactly coincides with that of the VED source located just below the surface if their moments M are related to each other as

$$(I\, dz\, h)_{\mathrm{VED}} = (I\, b^2/4)_{\mathrm{CED}} \tag{7}$$

and the following conditions are held:

$$h \ll r, |k_0 r| \ll 1, \text{ and } |\hat{\sigma}_1| \gg \varepsilon_0 \omega \left(k_j^2 = i\,\omega \hat{\sigma}_j \mu_0, \tilde{\sigma}_j = \sigma_j + i\,\omega \varepsilon_j\right). \tag{8}$$

Here, VED is located at depth $z = h$, and the equivalent CED is located on the surface, with an outer radius of b.

The vector potential for both sources on the surface of a half-space is described by the same equation $A_z = \frac{M}{2\pi}\frac{z}{R^3}(1 + k_1 R)\exp(-k_1 R)$, where $R = \sqrt{r^2 + z^2}$.

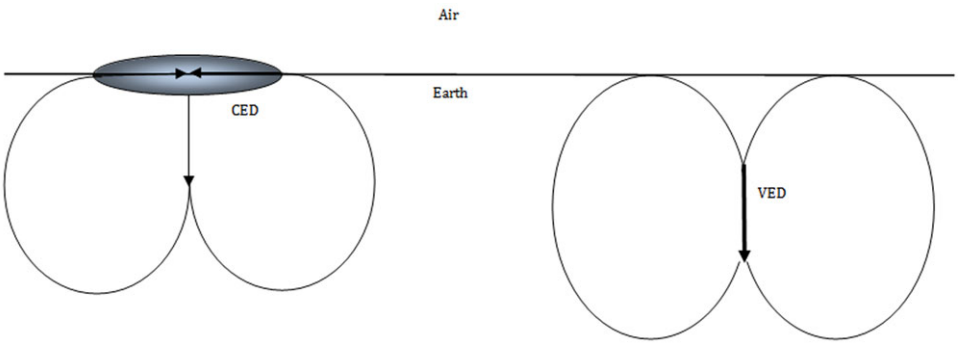

Figure 7 CED on the surface and VED below the surface of a half-space model.

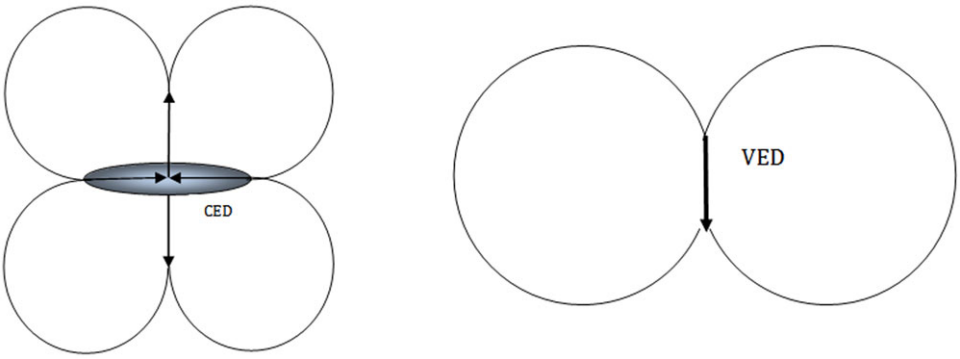

Figure 8 CED and VED within a full-space model.

This equation determines the geometry of the induced currents within the Earth and describes both sources as dipoles (Fig. 7).

However, if both sources are immersed deeply into the sea, the situation is drastically changed. The CED becomes a quadrupole with the above-mentioned vector potential in the vicinity of the source, whereas the VED, in complete accordance with its name, remains a dipole (Fig. 8) with the following vector potential in the vicinity of the source (Wait 1982):

$$A_z = \frac{Idz}{4\pi R}\mathrm{e}(-k_1 R) \tag{9}$$

Thus, the VED always forms just one toroidal current system, whereas the CED forms two current systems, i.e., upper and lower. The upper system disappears in the air when the CED is placed on the Earth's surface; then the VED and CED current systems become very similar. However, if the CED is placed deep in the sea, the VED and CED responses could become significantly different. This important point will be discussed in details in the modelling section.

The main shortcoming of the CED is the necessity to provide very stable and perfectly equal currents in all legs of the transmitter dipole. This is a very challenging problem in the case of large on-land transmitters, which can hardly be relocated during the survey. As a result, at present, the CED system is practically realized as on-land fixed transmitter mapping tool only (Mogilatov and Balashov 1996). As such, it realizes another remarkable feature of the VED/CED systems that is the complete absence of a magnetic field on the surface of 1D Earth. By distributing many magnetic field or electromotive force sensors (magnetometers or coils, respectively) within the area of interest, one can map lateral boundaries of the target using only one position of the transmitting CED. This is particularly important in on-land surveys, where relocating such a cumbersome transmitter is an extremely complicated technical problem.

Although the use of the vertical electric current soundings (VECS) method is practically preferable and even crucial in on-land surveys compared with the fixed-offset CED transient soundings, the latter seem to be more geophysically efficient by providing quantitative information regarding the resistivity distribution within the Earth. Moreover, similar to the above-discussed transient VED method, short-offset CED transient systems provide very high vertical and lateral resolutions under favourable conditions (see modelling section).

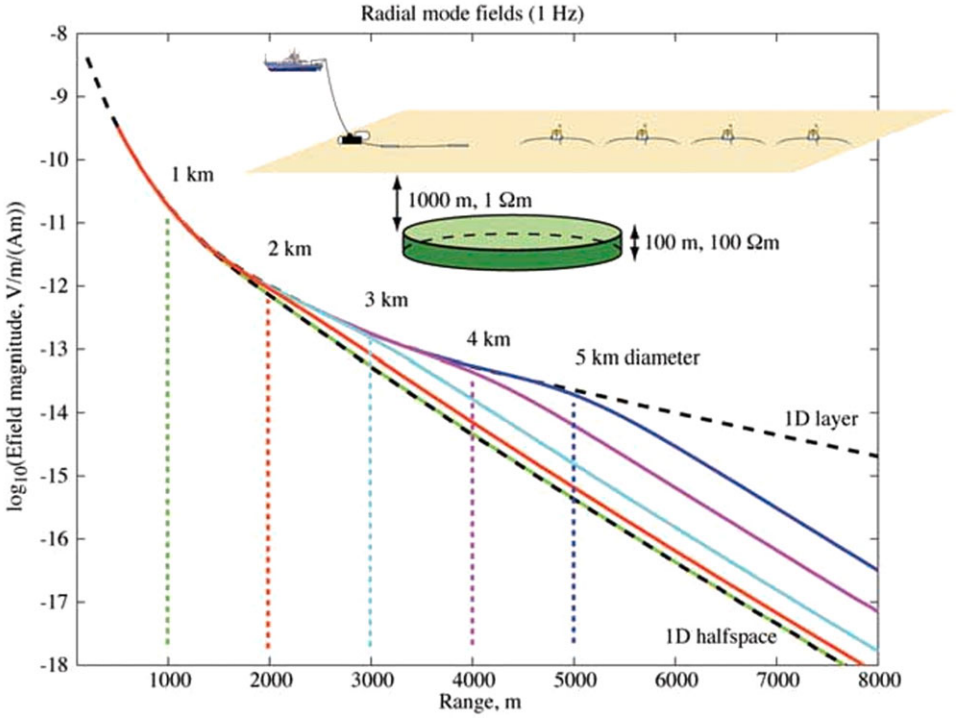

Figure 9 The CSEM response of a 3D disk of a variable diameter located at a depth of 1000 m within sub-seafloor sediments. The depth of the sea is 1 km, and the resistivity is 0.3 Ωm. The transmitter is positioned over the left edge of the disk. The working frequency is 1 Hz (Figure redrawn from Constable and Weiss (2006) by S. Constable (personal communication)).

Therefore, such systems seem to be feasible in marine environments, where the above-mentioned difficulties in providing stable equal currents in the radial legs of the CED are significantly simpler than on land. As for relocating CED transmitters in the sea, it strongly depends on the size of the transmitters. For shallow surveys, where rigid short-leg transmitters can be used, their relocation does not seem complicated. Relocating large CEDs, similar to those currently used in on-land VECS surveys ($b \sim 1$ km), could be a more complicated task than that for marine VED systems.

Thus, both the VED and CED represent a high-resolution alternative to the CSEM method in shallow sea and/or in the case of small lateral dimensions of the target (see the details in the modelling section). The choice between the VED and the CED solely depends on the above-mentioned technical difficulties and should be based on future practical experience with both methods.

MODELLING

In this section, the detectability of the above-mentioned methods with regard to a resistive sub-seafloor 3D target is studied using rigorous 3D forward modelling. Since the purpose of this study is a comparison of the methods and, particularly, of the novel techniques with the conventional CSEM method, the modelling is carried out for the classical 3D CSEM model shown in Fig. 9.

Since the studied model includes a single target, the detectability of a method virtually coincides with its lateral resolution. The latter will be studied here by fixing all geoelectric parameters of the target except lateral dimensions (the diameter). Figure 9 shows that, if the diameter of the disk does not exceed the depth of burial, the disk is virtually invisible. Taking into account inevitable distortions of the signal by ambient and, particularly, by geological noise, the minimum diameter of the disk to be reliably detected approaches to roughly three depths of burial.

Figure 10 shows the profiling curves of the transient VED and MCED arrays at fixed time and offset for the model similar to that shown in Fig. 9. The only difference between the models is in the shape of the target, which is represented here by a square slab having roughly the same area as the disk in Fig. 9. The difference in the shape is dictated by technical considerations (the simplicity of gridding) and does not play any

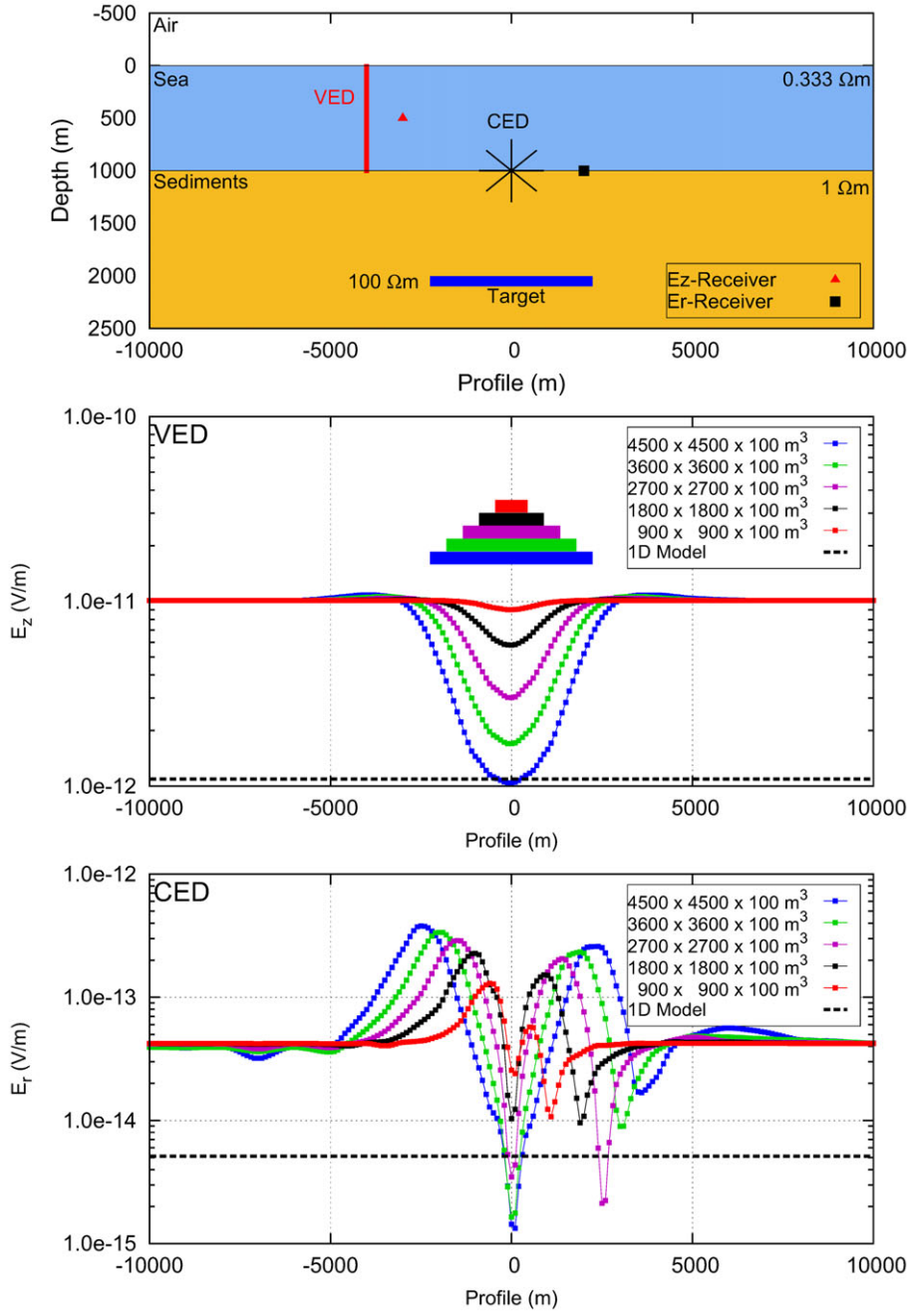

Figure 10 Deep sea profiling TDEM responses for Ez of VED and for Er of CED at fixed delay time of 10 s and 100 m and 200 m offsets, respectively. The model is shown in the upper panel. Different colors correspond to different lateral dimensions of the target. For visual clarity, the geometries in the upper panel are shown schematically and out of scale: The CED transmitter is shown as if it was located in the *xz* plane, whereas in reality, it is located in the *xy* plane, the offsets are exaggerated, etc.

significant role in the comparison (Goldman *et al.* 1994). The calculations for both VED and MCED systems were carried out using a modified spectral Lanczos decomposition method by Druzkin and Knizhnerman (1988). The CED transmitter was constructed using eight radial electric dipoles with a common central electrode (Fig. 6, left), as was previously recommended and practically realized by Mogilatov and Balashov (1996). The algorithm was verified by a comparison with 1D

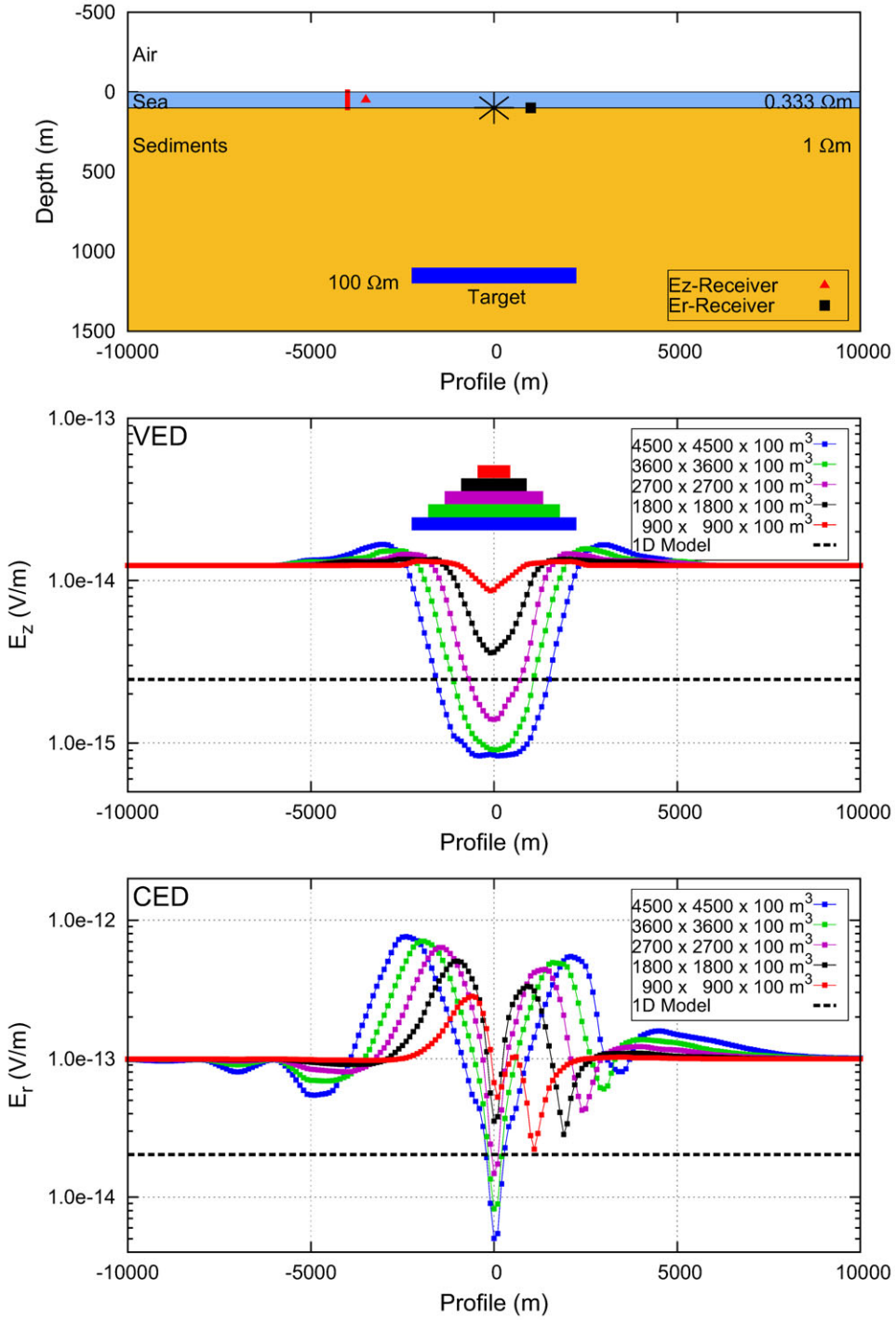

Figure 11 Shallow sea profiling TDEM responses. The depth of the sea is 100 m. The rest of the parameters and designations are identical to those in Fig. 10.

analytical solution for an arbitrarily located "ideal" CED and with the appropriate 3D calculations for a VED system, when both the VED and CED are located at the surface.

As it was predicted above, both the VED and CED provide an exceptionally high detectability (lateral resolution) compared with the long-offset CSEM method. The CED responses significantly differ from those of the VED. This is mainly caused by the different components used. As it was discussed above, with the VED transmitter, it is important to measure the Ez component. In the case of the bottom-located CED, it is not obvious what component could be measured more accurately. Therefore, a more efficient Er component has been selected for the analysis.

The comparison between VED(L) and CED(L) shows the following three distinguished features of the CED.

(i) The shape of the CED profiling responses fairly accurately follows the shape of the target. The responses have the maxima right above the edges of the body and the main minimum exactly above the center of the body. The additional extremum points reflecting the non-symmetrical geometry of the CED array represent artefacts and could pose certain problems in the interpretation, especially in the presence of 3D geologic noise. In contrast, due to the reciprocity principle, the responses of the VED are strictly symmetrical regarding the center of the target. They form a minimum above the center of the body, but the edges of the body are not clearly reflected in the VED responses.

(ii) The amplitudes of the CED responses above the edges significantly exceed the background values. This feature eliminates to a certain extent the Achilles' heel of all short-offset transient systems (and particularly those of the VED and CED), i.e., the SNR. The amplitudes of the VED responses are minimal above the body, thus making the signal-to-noise problem more severe.

(iii) The CED and VED target responses are similar for relatively large bodies (roughly three to four times larger than the depth of burial), but for small ones, the CED target responses are much greater than those of the VED. As a result, the CED exhibits a much higher detectability (lateral resolution) than the VED by being able to easily detect the target smaller than the depth of burial in the model under considerations. Such a target is hardly visible by VED and completely invisible by CSEM.

In the case of a shallow sea, the superiority of both VED and CED compared with CSEM becomes apparent. Figure 11 shows the profiling responses for VED and CED for a deep target in shallow sea. The detectability (lateral resolution) of both systems is very similar to that of the above-discussed deep sea. The amplitude of the VED responses drops significantly mainly because of the inevitably smaller size of the transmitter dipole. Therefore, at shallow sea, the CED has additional credit points compared with the VED as far as the SNR is concerned. This is in addition to the above-mentioned much higher detectability. As far as the CSEM method at shallow sea is concerned, the well-known air-wave limitation does not allow making use of the above-discussed propagation phenomenon. As a result, the greatest detectability is achieved in the LIN limits, and this reduces the detectability of the CSEM method to the level of a simple DC method, i.e., incomparably smaller than that of both the VED and, particularly, the CED.

DISCUSSION

It is shown that, despite significant difference in physical basics, the high detectability of all three methods considered in this study is based on common mathematical similarity. Under certain geoelectric conditions, the signals measured in these methods exponentially depend on geoelectric parameters of the Earth in the appropriate asymptotic domains. Such dependence leads to theoretically unlimited increase in the relative target response as a function of sounding parameters. The conditions and the asymptotic domain for the CSEM method are deep (theoretically infinitely deep) sea and HINs, respectively, whereas for the TEMP-VEL and MCED methods, these are highly resistive (theoretically insulating) target layer and late delay times. The appropriate sounding parameters are frequency (or offsets) for the CSEM method and delay times for the TEMP-VEL and MCED methods. In the case of all other (conventional) EM methods, the signals in asymptotic domains are changed as a power law of sounding parameters. As a result, the relative target response approaches some constant value, which theoretically limits the detectability of the method.

Of course, the above considerations represent only some theoretical framework, which requires further numerical and experimental substantiation. This is particularly true for the methods in question since the above-mentioned exponential decay of the signals in asymptotic domains leads to the abnormal smallness of the signals and as a result to the deteriorated signal-to-noise characteristics. Further limitations of the theoretically unlimited detectability are caused by a finite depth of the sea (CSEM) and by a finite resistivity of the target (TEMP-VEL and MCED). These important practical questions were investigated in great detail only for the CSEM method, in some detail for the TEMP-VEL method, and only theoretically for the MCED method.

CONCLUSIONS

The comparative analysis based on both previous investigations and analytical and numerical studies carried out in the framework of this research leads to the following conclusions.

(i) If lateral dimensions of a resistive sub-seafloor target, as well as the depth of the sea, are significantly greater than the depth to the target, then the standard Ex–Ex CSEM method is a preferable marine EM technique.

(ii) If the target is small, then either the TEMP-VEL or the MCED method should be applied in the deep sea, and the MCED method is preferable in the shallow sea. In both deep sea and shallow sea, the MCED method demonstrates better lateral resolution and signal-to-noise characteristics than a TEMP-VEL. However, contrary to the TEMP-VEL method, the feasibility of the MCED method has not yet been tested under real conditions.

(iii) In the shallow sea, irrespective to the size of the target, the application of the standard CSEM method is limited by the air-wave phenomenon. Although in special cases various mitigating techniques and the measurements at LINs might allow the CSEM method to resolve the target, the application of the TEMP-VEL method or the MCED method seems conceptually preferable. Due to the limited length of the transmitter dipole and particularly to severe non-verticality issues in the TEMP-VEL method (Appendix B), the MCED method seems more promising, although its practical feasibility is still questionable.

ACKNOWLEDGEMENTS

The authors would like to thank James Macnae and the anonymous reviewer for numerous extremely useful comments and corrections. Figure 9 in this article was reproduced with kind permission of Steven Constable. The authors would like to thank Carsten Scholl for the permission to use his 1D forward modelling code.

REFERENCES

Alumbaugh D., Cuevas N.H., Chen J., Gao G. and Brady J. 2010. Comparison of sensitivity and resolution with two marine CSEM exploration methods. 80th SEG Annual Meeting, Denver, Colorado, Expanded Abstracts, 3893–3896.

Chave A.D. and Cox C.S. 1982. Controlled electromagnetic sources for measuring electrical conductivity beneath the oceans: Part 1—Forward problem and model study. *Journal of Geophysical Research* **87**, 5327–5338.

Chave, A.D. 2009. On the electromagnetic fields produced by marine frequency domain controlled sources. *Geophysical Journal International* **179**, 1429–1457.

Commer M. and Newman G. 2008. New advances in three-dimensional controlled-source electromagnetic inversion. *Geophysical Journal Inter-national* **172**, 513–535.

Connell D. and Key K. 2013. A numerical comparison of time and frequency-domain marine electromagnetic methods for hydrocarbon exploration in shallow water. *Geophysical Prospecting* **61**, 187–199.

Constable S. 2006. Marine electromagnetic methods—A new tool for offshore exploration. *The Leading Edge* **25**, 438–444.

Constable S. 2010. Ten years of marine CSEM for hydrocarbon exploration. *Geophysics* **75**, 75A67–75A81

Constable S. and Srnka L.J. 2007. An introduction to marine controlled source electromagnetic methods for hydrocarbon exploration. *Geophys-ics* **72**, WA3–WA12.

Constable S. and Weiss C.J. 2006. Mapping thin resistors and hydrocar-bons with marine EM methods: Insights from 1D modeling. *Geophysics* **71**, G43–G51.

Cox C.S. 1981. On the electrical conductivity of the oceanic lithosphere. *Physics of the Earth and Planetary Interiors* **25**, 196–201.

Cuevas N.H. and Alumbaugh D. 2011. Near-source response of a resistive layer to a vertical or horizontal electric dipole excitation. *Geophysics* **76**, F353–F371.

Druskin V.L. and Knizhnerman L.A. 1988. A spectral semi-discrete method for the numerical solution of three-dimensional nonstationary electrical prospecting problems. *Izvestiya, Physics of the Solid Earth* **8**, 63–74.

Edwards N. 2005. Marine controlled source electromagnetics: principles, methodologies, future commercial applications. *Surveys in Geophysics* **26**, 675–700.

Edwards R.N., Law L.K. and DeLaurier J.M. 1981. On measuring the electrical conductivity of the ocean crust by a modified magnetometric resistivity method. *Journal of Geophysical Research* **86**, 11609–11615.

Edwards R.N., Law L.K., Wolfgram P.A., Nobes D.C., Bone M.N., Trigg D.F. *et al.* 1985. First results of the MOSES experiment: sea sediment conductivity and thickness determination, bute inlet, British Columbia, by magneto-metric off-shore electrical sounding. *Geophysics* **50**, 153–160.

Ellingsrud S., Eidesmo T., Johansen S., Sinha M.C., MacGregor L.M. and Constable S.C. 2002. Remote sensing of hydrocarbon layers by seabed imaging (SBL): results from a cruise offshore Angola. *The Leading Edge* **21**, 972–982.

Goldman M. 1983. The integral-finite-difference method for calculating transient electromagnetic fields in a horizontally stratified medium. *Geophysical Prospecting* **31**, 664–686.

Goldman M. 1987. Forward modelling for frequency domain marine electromagnetic systems. *Geophysical Prospecting* **35**, 1042–1064.

Goldman M. 1990. *Non-Conventional Methods in Geoelectrical Prospecting*. Ellis Horwood Ltd.

Goldman M. and Fitterman D. 1987. Direct time-domain calculation of the transient response for a rectangular loop over a two-layered medium. *Geophysics* **52**, 997–1006.

Goldman M., Levi E., Tezkan B. and Yogeshwar, P. 2011. The 2D coastal effect on marine time domain electromagnetic measurements using broadside dBz/dt of an electrical transmitter dipole. *Geophysics* **76**, F101–F109.

Goldman M. and Mogilatov V. 1978. Transient field of a vertical electric dipole embedded in a horizontally layered half-space (in Russian). In: *Theory and Applications of Electromagnetic Fields in Geophysical Exploration*. Academy of Science of the USSR, Siberian Branch, 123–138.

Goldman M, Tabarovsky L. and Rabinovich M. 1994. On the influence of three-dimensional structures in the interpretation of transient electromagnetic sounding data. *Geophysics* **59**, 889–901.

Holladay J.S. 1981. YVESFT and CHANNEL, A Subroutine Package for Stable Transformation of Sparse Frequency Domain Electromagnetic Data to the Time Domain. *Research in Applied Geophysics* **17**, Geophysics Laboratory, University of Toronto.

Holten T., Flekkøy E.G., Måløy K.J. and Singer B. 2009. Vertical source and receiver CSEM method in time-domain. 79th SEG Annual Meeting, Houston, Texas, Expanded Abstracts, 749–752.

Kaufman A. 1978. Frequency and transient responses of electromagnetic fields created by currents in confined conductors. *Geophysics* **43**, 1002–1010.

Kaufman A., Goldman M., Lee D.S. and Keller G. 1981. Marine electromagnetic prospecting system. 51st SEG Annual Meeting, Abstracts and Biographies, 21.

Kaufman A.A. and Keller G.V. 1983. *Frequency and transient soundings*. Elsevier Science Publishers B.V.

Key K. 2009. 1D inversion of multicomponent, multifrequency marine CSEM data: Methodology and synthetic studies for resolving thin resistive layers. *Geophysics* **74**, F9–F20.

Loseth L.O. and Amundsen L. 2007. On the signal propagation in marine CSEM. 69th EAGE Conference and Exhibition, Extended Abstracts, D035.

Mogilatov V. 1992. A circular electric dipole as a new source in electric surveys. *Izvestiya, Physics of the Solid Earth* **6**, 97–105.

Mogilatov V. 1996. Excitation of a half-space by a radial current sheet source. *Pure and Applied Geophysics* **14**(7), 763–775.

Mogilatov V. and Balashov B. 1996. A new method of geoelectrical prospecting by vertical electric current soundings. *Journal of Applied Geophysics* **36**, 31–41.

Nazarenko O. 1961. *Electrical device for marine exploration*. USSR patent 751834/26–10.

Scholl C. and Edwards R.N. 2007. Marine downhole to seafloor dipole-dipole electromagnetic methods and the resolution of resistive targets. *Geophysics* **72**, WA39–WA49.

Singer B.S. and Atramonova S. 2013. Vertical electric source in transient marine CSEM: Effect of 3D inhomogeneities on the late time response. *Geophysics* **78**, E173–E188.

Stolz E.M. and Macnae J. 1998. Evaluating EM waveforms by singular- value decomposition of exponential basis functions. *Geophysics* **63**, 64–74.

Tikhonov A.N. 1950. On transient electric currents in an inhomogeneous layered medium. *Izvestiya, Physics of the Solid Earth* **14**.

Um E.S. and Alumbaugh D.L. 2007. On the physics of the marine controlled-source electromagnetic method. *Geophysics* **72**, WA13–WA26.

Um E.S., Alumbaugh D.L., Harris J.M. and Chen J. 2012. Numerical modeling analysis of short-offset electric-field measurements with a vertical electric dipole source in complex offshore environments. *Geophysics* **77**, E329–E341.

Wait J.R. 1982. *Geo-Electromagnetism*. Academic Press.

Weidelt P. 2007. Guided waves in marine CSEM. *Geophysical Journal International* **171**, 153–176.

Weiss C.J. and Constable S. 2006. Mapping thin resistors and hydrocar-bons with marine EM methods: Part 2—Modeling and analysis in 3D. *Geophysics* **71**, G321–G332.

APPENDIX A
TRANSIENT FIELD OF A VERTICAL ELECTRIC DIPOLE WITHIN CONDUCTIVE SLAB

Let us consider a two-layer model with an insulating basement (Fig. A1).

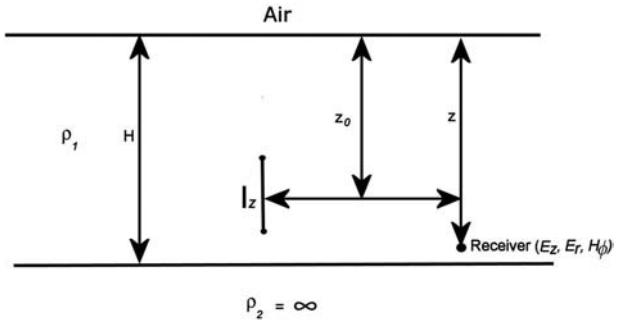

Figure A1 The slab model used to formulate the boundary value problem directly in the time domain.

The upper layer ($\rho_1, 0 \le z \le H$) is isotropic and non-magnetic. The VED transmitter is located within the layer at $z = z_0$ and has a moment $I_z = Idz$, where I is a current in the transmitter before switch off. Using a cylindrical coordinate system, the Maxwell's equations for the only non-zero field components (E_r, E_z, and H_ϕ) within the layer can be represented in the quasistatic approximation as follows:

$$-\frac{\partial H_\varphi}{\partial z} = \frac{E_r}{\rho_1}, \quad \frac{1}{r}\frac{\partial (r H_\varphi)}{\partial r} = \frac{E_z}{\rho_1}, \quad \frac{\partial E_r}{\partial z} - \frac{\partial E_z}{\partial r} = -\mu_0 \frac{H_\varphi}{\partial t}, \quad \frac{1}{r}\frac{\partial (r E_r)}{\partial r} + \frac{\partial E_z}{\partial z} = 0. \tag{A1}$$

By separating the variables, the solution can be represented as

$$\begin{aligned} H_\varphi &= \tfrac{I_z}{4\pi} \int_0^\infty J_1(\lambda r)\lambda V(z,t,\lambda)d\lambda, \\ E_r &= -\tfrac{I_z \rho_1}{4\pi} \int_0^\infty J_1(\lambda r)\lambda V_z'(z,t,\lambda)d\lambda, \\ E_z &= \tfrac{I_z \rho_1}{4\pi} \int_0^\infty J_0(\lambda r)\lambda^2 V(z,t,\lambda)d\lambda. \end{aligned} \tag{A2}$$

For the unknown function V, the following boundary value problem can be formulated after switching off the transmitter current within $0 \le z \le H$:

$$\begin{cases} \frac{\partial^2 V}{\partial z^2} - \lambda^2 V = \frac{\mu_0}{\rho_1}\frac{\partial V}{\partial t}, \quad 0 < z < H, \\ V = 0, z = 0, H, \\ V = \overline{V}(\lambda, z), t = 0, \\ V \to 0, t \to \infty. \end{cases} \tag{A3}$$

Here, $\overline{V}(\lambda, z)$ is the DC solution satisfying the following boundary value problem:

$$\begin{cases} \overline{V}'_{zz} - \lambda^2 \overline{V} = 0, 0 \le z \le H, \\ \overline{V} = 0, z = 0, H, \\ [\overline{V}]\big|_{z=z_0} = 0, [\overline{V}_{z'}]\big|_{z=z_0} = 2\lambda, \end{cases} \tag{A4}$$

where the latter conditions at $z = z_0$ are obtained from the known expression of the magnetic field near the transmitter (Biot–Savart law):

$$H_\varphi = \frac{I_z}{4\pi}\frac{r}{\left[r^2 + (z - z_0)^2\right]^{3/2}} \equiv \frac{I_z}{4\pi}\int_0^\infty J_1(\lambda r)\lambda \exp(-\lambda|z - z_0|)d\lambda.$$

By further separating variables in equation (A3), the solution for function V can be sought in the form $V \approx \zeta(z)\exp(-\alpha t)$. Finally, for the auxiliary function ζ, the following simple boundary value problem is formulated:

$$\begin{cases} \zeta''_{zz} + (\alpha\mu_0/\rho_1 - \lambda^2)\zeta = 0, 0 < z < H, \\ \zeta = 0, z = 0, H, \end{cases} . \tag{A5}$$

The solution to this problem is an infinite sequence $\zeta_k = \sin(k\pi z/H), \quad k = 1, 2, 3, \ldots$ with $\alpha_k = (\frac{k^2\pi^2}{H^2} + \lambda^2)\frac{\rho_1}{\mu_0}$. Thus, the general solution for V can be represented as a series

$$V = \sum_{k=0}^{\infty} C_k \zeta_k(z)\exp(-\alpha_k t), \tag{A6}$$

Coefficients C_k are determined by satisfying the initial condition for function V. Considering equation (A6) at $t = 0$ and using the orthogonality feature of $\zeta_k$within $0 \le z \le H$, one obtains

$$C_k = \frac{\int_0^H \overline{V}(z)\zeta_k(z)dz}{\int_0^H \zeta_k^2(z)dz} = \frac{4\lambda\rho_1}{H\mu_0}\frac{\sin(k\pi z_0/H)}{\alpha_k},$$

Thus, the final solutions for the field components directly in the time domain are represented by the following equations:

$$\begin{aligned} H_\varphi &= \frac{I_z}{\pi H^2}\sum_{k=1}^{\infty} e^{-k^2\pi^2\bar{t}}\sin(k\pi\bar{z})\int_0^\infty R_k e^{-\lambda^2\bar{t}}\lambda J_1(\lambda\bar{r})d\lambda, \\ E_r &= -\frac{I_z\rho_1}{H^3}\sum_{k=1}^{\infty} e^{-k^2\pi^2\bar{t}}k\cos(k\pi\bar{z})\int_0^\infty R_k e^{-\lambda^2\bar{t}}\lambda J_1(\lambda\bar{r})d\lambda, \\ E_z &= \frac{I_z\rho_1}{\pi H^3}\sum_{k=1}^{\infty} e^{-k^2\pi^2\bar{t}}\sin(k\pi\bar{z})\int_0^\infty R_k e^{-\lambda^2\bar{t}}\lambda^2 J_0(\lambda\bar{r})d\lambda, \end{aligned} \tag{A7}$$

where

$$R_k = \frac{\lambda\sin(k\pi z_0/H)}{\lambda^2 + k^2\pi^2}, \quad \bar{t} = \frac{t\rho_1}{\mu_0 H^2}, \quad \bar{r} = \frac{r}{H}, \quad \bar{z} = \frac{z}{H}.$$

APPENDIX B
THE INFLUENCE OF NON-VERTICALITY OF A VERTICAL ELECTRIC DIPOLE

Under ideal ocean conditions (no waves, winds, currents, etc.), the assembly of a VED in the marine environment is expected to be much more efficient compared with the assembly of a CED, particularly if the latter is being placed at the sea bottom. However, under real conditions, the verticality of the VED transmitter and Ez receivers becomes a vulnerable issue.

Figure B1 demonstrates that a VED inclination of angle ϕ causes the appearance of a HED with the length

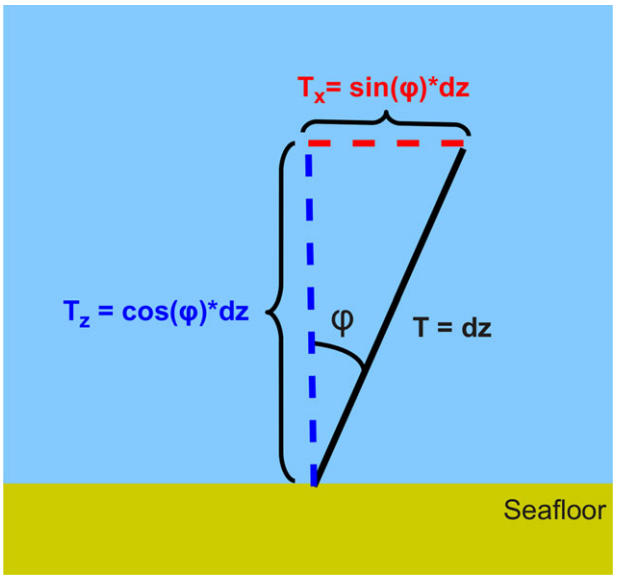

Figure B1 Setup of a VED transmitter at angle ϕ. Due to the inclination of the VED transmitter, a horizontal transmitter component (Tx) with the length $Tx = \sin(\phi)dz$ appears.

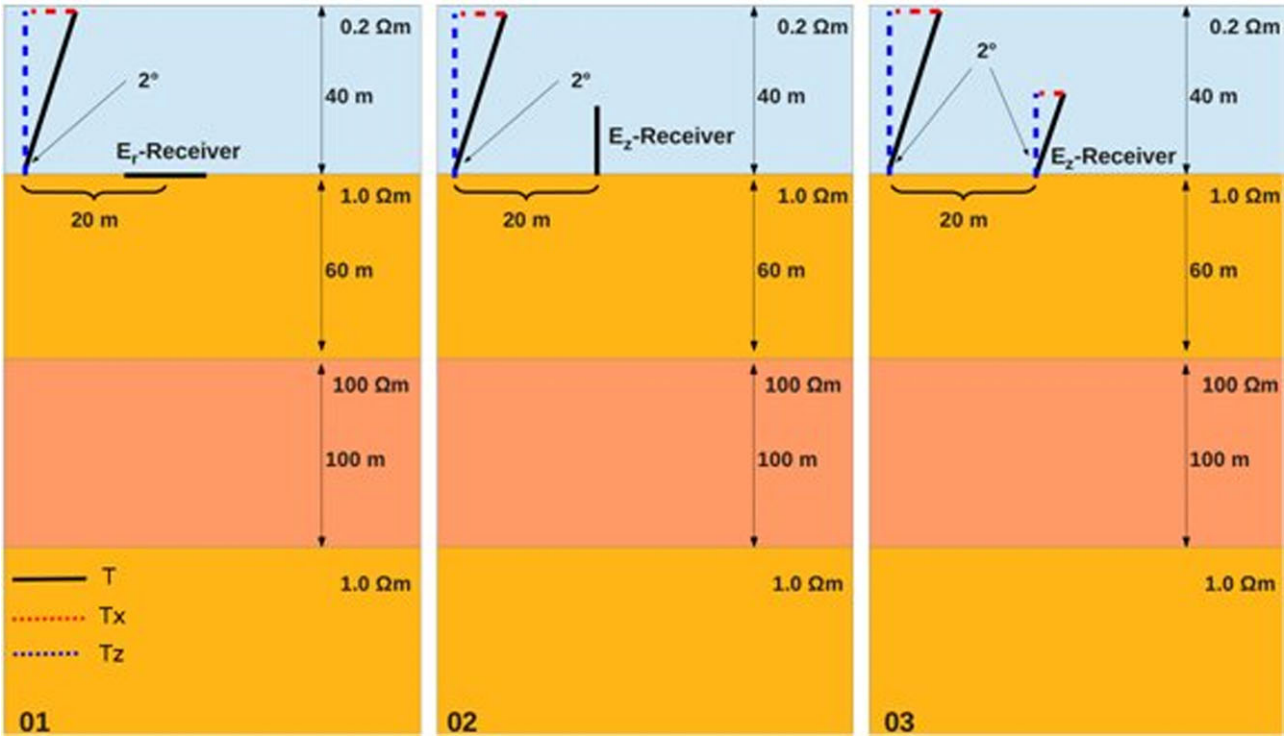

Figure B2 The parasitic effect of the horizontal transmitter component from a VED inclined at an angle of 2°. The 1D resistivity model represents a sub-seafloor fresh groundwater aquifer with a thickness of 100 m and a resistivity of 100 Ωm embedded in marine sediments with a resistivity of 1 Ωm. The sea has a resistivity of 0.2 Ωm (Mediterranean Sea) and a depth of 40 m. The receivers are both horizontal (01) vertical (02) and inclined (03).

$Tx = \sin(\phi)dz$. This horizontal transmitter component generates an EM field, which decays much slower than that of an ideal VED. For example, in the case of an insulating basement, the VED signal decays exponentially with time, whereas the HED signal decays as a power of time (Goldman 1990). Therefore, even a small HED component may generate a parasitic field with a signal comparable or even much greater than the required field of a VED transmitter.

To investigate this effect on different Tx–Rx configurations, 1D resistivity models corresponding to an offshore fresh groundwater hydrogeological model were investigated. A high-resistivity fresh groundwater aquifer (100 Ωm) with a thickness of 100 m is embedded in marine sediments (1 Ωm) at a depth of 60 m beneath the seafloor. Figure B1 shows the investigated Tx–Rx configurations. In Fig A2–01, a VED transmitter at an angle of 2° with an Er receiver is displayed. Figs. B2–02 and B2–03 show the same transmitter with an Ez receiver, which also has an inclination angle of 2° in Fig. B2–03.

The corresponding transients of Fig. B2 are displayed in Fig. B3. The blue line represents the signal of the vertical component (Tz) of the inclined VED. Since $\cos(2°)\,dz \approx dz$, the blue line is almost identical to the signal of an ideal VED. The red line represents the signal caused by the horizontal transmitter component $Tx = \sin(2°)dz$, whereas the black line is the actual signal due to the inclined VED transmitter.

Figure B3–01 clearly demonstrates that the use of a horizontal receiver with a VED transmitter leads to severe errors in the intermediate and late times, where the signal is completely dominated by the parasitic horizontal dipole Tx. An interpretation of such strongly distorted transients will lead to a completely wrong subsurface resistivity distribution.

The second configuration (Fig. B2–02) assumes that the VED transmitter is slightly non-vertical (again 2°), but the Ez receiver is perfectly vertical. For this case, the non-verticality of the transmitter has very little influence on the measured

signal (Fig. A3–02). The parasitic effect, caused by the HED transmitter component, only influences the signal at very early times. Throughout the rest of the transient response (especially at the late times), this effect is roughly by two orders of magnitude less than that of an ideal VED. This is the reason why the real TEMP-VEL system utilizes both transmitter and receiver vertical lines (Holten *et al.* 2009).

However, it is reasonable to assume that a perfectly vertical receiver is almost just as difficult to assemble as the transmitter, and the realistic array is therefore represented by two inclined electric dipoles (Fig. B2–03). It is not clear whether the conditions leading to non-verticality will have the same effect on the transmitter and the receiver, but for simplicity, we assume that this is the case. Thus, suppose both vertical transmitter and receiver dipoles are inclined by the same angle of 2°. The corresponding transient responses are displayed in Fig. B3–03. It should be noted that another two Tx–Rx components (Tx–Ez and Tz–Ex) also exist in this setting, but they are not displayed since their effect is negligible. Again, the strong parasitic effect caused by the HED transmitter component significantly influences the signal at late times. At approximately 10 ms, the inclined VED transient is strongly affected by the HED component. In comparison to the Ex-receiver transient exhibited in Fig. B3–01, the parasitic effect for this setting is significantly lower by the factor of sin(2°). Therefore, the effect becomes relevant at much later times, but still it might lead to a misinterpretation of the true resistivity model if these times are significant for the interpretation.

This modelling study proves that non-verticality of the VED transmitter and/or receiver poses a severe problem especially in shallow marine environments, where even small deviations of the surface dipole lead to significant inclination angles.

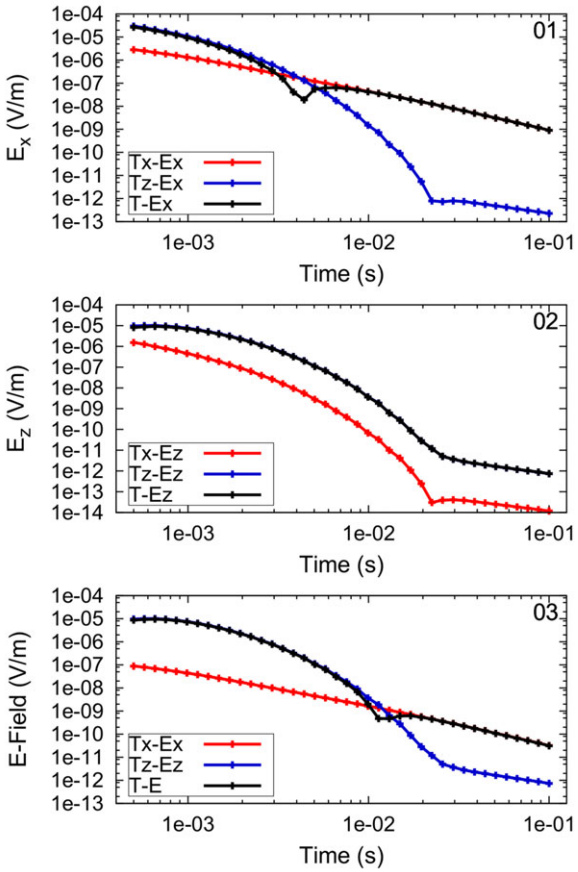

Figure B3 Electrical field transients of the different components according to the three configurations of Fig. B2. The top image (01) illustrates the Ex transient of the horizontal transmitter component (Tx) in red, the Ex transient of the vertical transmitter component (Tz) in blue, and the transient of the total slanted VED transmitter (T) in black. Image 02 shows the Ez transients of all above-mentioned transmitter components, and image 03 shows the Ex component of the Tx transmitter component along with the Ez component of the Tz transmitter component. The combined transient is again shown in black.